Proceedings of the 17th World Congress
The International Federation of Automatic Control
Seoul, Korea, July 6-11, 2008

Closed-loop Individual Cylinder Air-Fuel Ratio Control via UEGO Signal Spectral Analysis

Nicolò Cavina*, Enrico Corti*, Davide Moro*

**DIEM – University of Bologna, Italy*
(Tel: +39-051-2093307/09; e-mail: nicolo.cavina@unibo.it, enrico.corti2@unibo.it, davide.moro@unibo.it).

Abstract: The paper presents the development and real time application of an original closed-loop individual cylinder AFR control system, based on a spectral analysis of the lambda sensor signal measured at the confluence of the various exhaust runners. The observation that any type of AFR disparity between the various cylinders is reflected in a specific harmonic content of the AFR signal spectrum, represents the starting point of the project. The proposed approach has been designed in order to be compatible with on-board application. The AFR individual cylinder closed-loop controller has been tested in real time, by implementing it in a virtual Electronic Control Unit, using rapid control prototyping techniques. The results observed on a 4 cylinder Spark Ignition 1.2 liter engine are encouraging, since in the investigated engine operating conditions the controller is able to guarantee AFR inequality below 0.01 lambda. The paper shows how the proposed controller can be applied to other engine configurations (6, 8, or 12 cylinder engines), if a lambda sensor is available per each engine bank.

1. INTRODUCTION

Typical Spark Ignition (SI) engines Air-to-Fuel Ratio (AFR) control systems allow excellent steady-state mean performance, guaranteeing for example that the gas flow exhausted by the engine can be controlled at a desired lambda value in its average composition. Cylinder-to-cylinder AFR variations are usually not compensated both in the open-loop part of the control structure, nor in the closed-loop, lambda-measurement based correction.

On one hand, such variations may be large and could effectively influence fuel consumption, emissions and torque production (Kainz *et al*., 1999, Grizzle *et al*., 1991, Colvin *et al*., 1999). On the other, since the main reason for unbalanced AFR values can be found in uneven air charge distribution, and/or injector characteristic dispersion (Kainz *et al*., 1999), the solution for reducing such AFR disparity could be twofold:

- Cylinder-to-cylinder injection time compensation maps can be experimentally identified (by installing one lambda sensor for each exhaust runner during the identification phase) and inserted in the open-loop AFR control strategy.
- Closed-loop cylinder-by-cylinder AFR control algorithms could be developed to be run in parallel with the existing closed-loop engine-averaged correction.

While the first solution would require a significant experimental effort (especially for the most recent SI engines, where the cylinder-to-cylinder AFR disparity may be influenced by several factors such as Variable Valve Timing configuration, external Exhaust Gas Recirculation, canister purging strategy, intake/exhaust variable geometry manifolds, tumble/swirl control devices, …), as it is well-known the closed-loop approach cannot be based on monitoring each cylinder exhaust gas composition by installing one lambda sensor in each exhaust runner, essentially for cost reasons. Usually, in fact, a single lambda sensor (in most recent powertrains a linear oxygen sensor – or UEGO – is normally used) is installed at the confluence of each engine bank. The limited bandwidth of typical UEGO-based AFR measuring systems, and the usually nonlinear gas transport and mixing phenomena that take place in the exhaust manifold, have allowed to provide a control feedback limited to the average (or "engine") AFR deviation from the set-point (which is converted into an injection time correction that is identical for all the engine cylinders, on a cycle-by-cycle basis).

As already mentioned, although the average AFR may be for example controlled to achieve stoichiometry, individual cylinders may be operating consistently richer or leaner than the desired value (± 0.7 AFR is reported in (Kainz *et al*., 1999) as a reasonable range for engine overall AFR disparity), and such observation leads to the conclusion that by reducing such type of unbalances, both fuel consumption and maximum output torque can be effectively improved (Kainz *et al*., 1999). Moreover, reducing cylinder-by-cylinder torque production irregularity improves cabin comfort, especially at idle. One further positive aspect of individual cylinder AFR control would be a significant cost reduction for the fuel injectors, by allowing larger tolerances (in terms of injected mass versus injection time) during the component machining and assembly process (Grizzle *et al*., 1991, Benvenuti *et al*., 2003). Last but not least, catalyst performance would be optimized by feeding it with more uniform gas composition, thus reducing tailpipe emissions.

The paper presents an original way of dealing with this situation, through the development and real time application

of a single-UEGO based closed-loop individual cylinder AFR control system, based on a spectral analysis of the lambda sensor signal. In the following sections the proposed approach will be briefly presented, then the experimental setup used to verify and validate the control structure will be described, and finally some results that have been obtained by implementing it in a virtual Electronic Control Unit, using rapid control prototyping techniques, will be shown and discussed. It should also be highlighted the fact that the proposed approach should in principle be applicable to exhaust configurations that present linear (UEGO) or nonlinear (EGO) lambda sensors, being the latter limited to closed-loop control of stoichiometric mixture. Finally, the proposed controller can be applied to any automotive engine (Spark Ignition and Compression Ignition) exhaust configuration, being the V12 the most challenging one and the V6 (or L3) the easiest case.

2. METHODOLOGY

Several researchers have recently devoted their attention to the design of closed-loop lambda-based control systems, able to compensate for cylinder-to-cylinder AFR deviations (Kainz *et al*., 1999, Hasegawa *et al*., 1994, Carnevale *et al*., 1998, Fantini *et al*., 2000, Fantini *et al*., 2003, Bush *et al*., 1994). Most of the proposed approaches are based on the development of a simplified model for exhaust transport, mixing phenomena, and sensor dynamics. An observer is then applied to the model, in order to perform real-time state estimation, for example by using Kalman filter theory (Hasegawa *et al*., 1994, Carnevale *et al*., 1998, Fantini *et al*., 2000, 2003). The ability to estimate each cylinder AFR would allow for accurate and perfectly stable AFR uniformity, but the main drawbacks of such approach are the need for long and expensive experimental tests (to identify several exhaust dynamics model unknown parameters), and the large influence that sensor bandwidth (and especially its variation with sensor ageing) and sensor installation position have on the overall system performance.

The proposed approach is instead based on the analysis of the frequency content of the confluence UEGO signal, in particular by using off-the-shelf UEGO controllers with large bandwidth output (the voltage output by the controller is proportional to the pumping current flowing in and out of the sensor (Naito *et al*., 2001)). The main observation upon which this work is based is that any type of AFR uneven distribution should be reflected into few and specific frequencies of the AFR signal spectrum measured at the runners confluence point. Therefore, a controller able to reduce the amplitude of the AFR signal spectrum at those specific frequencies would necessarily reduce the AFR disparity. This, together with a slower AFR engine (or bank) mean value closed-loop controller to be run in parallel, would allow reducing cylinder-by-cylinder AFR variations while guaranteeing the same AFR mean value.

For example, for a 4 in 1 exhaust manifold confluence system, any type of AFR difference in the flows coming from the exhaust runners will necessarily be reflected onto the engine cycle frequency amplitude value of the confluence lambda signal, and/or onto its first harmonic (crankshaft rotation frequency). In the next paragraphs it will be demonstrated that the number and type of specific frequencies over which a signature of the AFR distribution can be found, strictly depends on the number of exhaust runners that are connected to the same confluence point (if the combustion phases of the various cylinders are evenly distributed within the engine cycle).

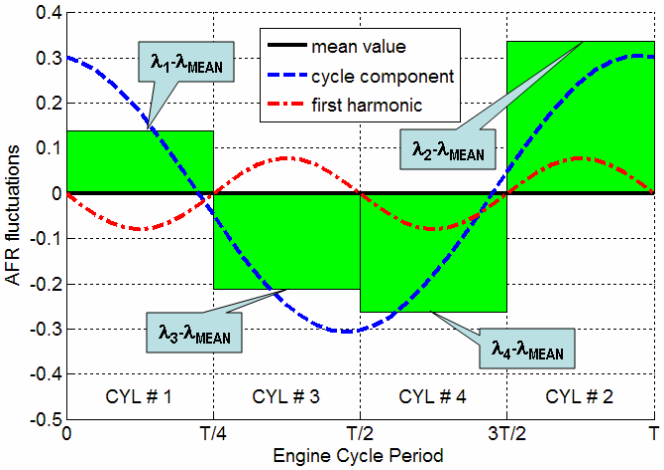

Fig. 1. AFR oscillations of a virtual confluence signal. Decomposition into cycle and first harmonic frequency components.

By considering a 4 cylinder engine with firing order 1-3-4-2, Figure 1 shows a simplified model that helps understanding the preceding assertions. If we consider a signal being composed of the individual cylinders AFR signals, each of them windowed during that specific cylinder exhaust stroke, we can obtain a virtual AFR signal that could be measured by an ideal sensor (unlimited bandwidth) if no transport and no mixing took place. Once we subtract the cycle mean value from such virtual signal, we would get the sequence of AFR constant steps as the one shown in Figure 1, if the various cylinders did present that specific AFR distribution (the type of hypothesized AFR distribution is not really important here, since the main purpose is to identify the correspondence between any given AFR distribution and the unique features of the corresponding AFR signal spectrum).

As it can be observed in Figure 2, such AFR fluctuation can be first of all decomposed into two specific frequency components: the one corresponding to the cycle frequency, and the one corresponding to the crankshaft rotation frequency (first harmonic of the previous one). Moreover, the knowledge of the amplitude and phase of these two frequency components of the signal spectrum would allow the controller to univocally reconstruct any type of AFR fluctuations with respect to the overall mean value, as it will be shown in the next section. This consideration leads to the conclusion that an individual cylinder AFR closed-loop observer could be designed by correctly estimating such parameters (amplitude and phase of the interesting frequency components) in real time, but even more interesting is the fact that a closed-loop individual AFR controller designed to re-establish AFR uniformity would only need as input the "shape" of the AFR distribution (i.e., the phase). That information would in fact

be sufficient to generate error inputs to feed a number of Proportional-Integral (PI) controllers equal to the number of the engine cylinders. Given these remarks, it should be observed that for a 4 cylinder engine any AFR distribution may be thought as being due to the sum of two independent contributions. As shown in Figure 2, in fact, the overall AFR distribution can be regarded as being due to the sum of a cycle frequency pattern and of a first harmonic pattern.

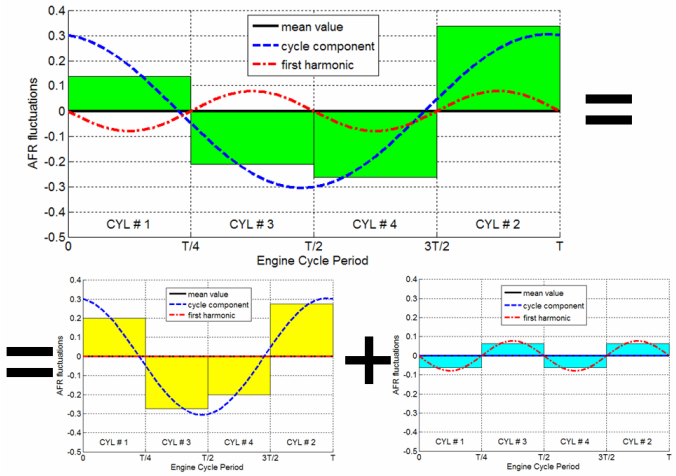

Fig. 2. AFR oscillations of a virtual confluence signal. Decomposition into cycle and first harmonic AFR distribution patterns.

For a 4 in 1 exhaust manifold confluence system, the design of a closed-loop individual cylinder AFR controller could be therefore based on the continuous monitoring of the amplitude of the two interesting frequency components, and on a number of PI elements (one for each cylinder and for each frequency component) whose purpose is the reduction of the very same amplitudes. In fact, if the amplitude of both such frequency components is equal to zero, the AFRs of the various cylinders are necessarily identical.

Some considerations should be made before proceeding to describe the mathematical aspects of the proposed approach:

- It should be demonstrated that the proposed signal processing technique can still recover the main characteristics of the interesting frequency components, even when all the hypothesis introduced at the beginning of this section (no mixing, no transport delay, ideal sensor) no longer hold, as in a typical exhaust system architecture.
- If the main effects of mixing, gas transport, and sensor limited bandwidth on the signal spectrum are amplitude reduction and phase shift of the interesting frequency components, the only information needed to implement the proposed strategy is the phase shift (induced by the system geometry, exhaust gas flow characteristics, and sensor Frequency Response Function). For a given engine-sensor layout, such information may be experimentally determined by applying pre-defined patterns to the various cylinder injection times, for every speed-load breakpoint, and by mapping the corresponding phase delay.

3. SIGNAL PROCESSING

The first step in order to test the methodology feasibility is briefly described in the following paragraphs. A preliminary study was in fact performed to understand both whether the above-mentioned phenomena still allow a sufficiently robust frequency content extraction, and to verify if the phase delay could be identified in a simple and straightforward way. A set of data previously acquired was used for this purpose, in which specific injection patterns where induced in a 1.4 liter, 4 cylinder Gasoline Direct Injection engine under steady-state conditions, after having installed one UEGO sensor in each exhaust runner and one at the runners confluence point. An example of such injection time (and lambda) perturbations is shown in Figure 3, while the engine was running at 3000 rpm and at a load level corresponding to 0.6 bar of intake manifold pressure. As shown in the figure, the first AFR perturbation involved all the engine cylinders, while the subsequent ones where applied to the various cylinders, one at a time.

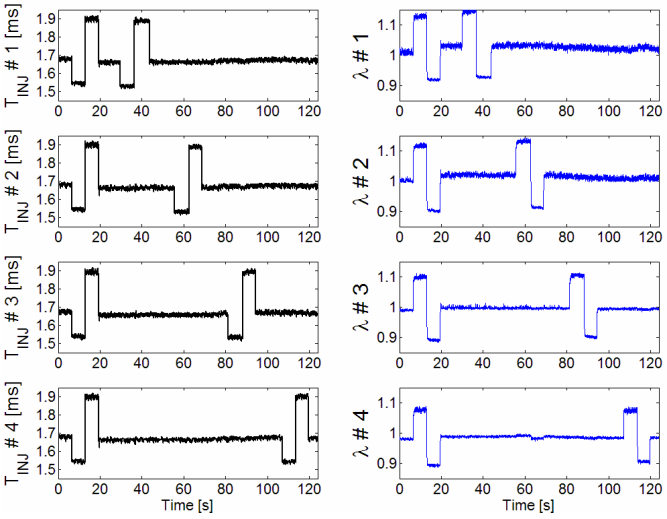

Fig. 3. AFR perturbation tests. Both injection time and UEGO measured lambda trends are reported for each engine cylinder.

The analysis of such experimental data was then conducted offline, to first of all verify whether the interesting features (phase and amplitude of specific frequency components) of the confluence signal spectrum could be effectively extracted, and to better understand how the control strategy described above could be implemented in real time.

The confluence signal (λ_{confl}) was pre-processed in order to recover the interesting part of its frequency content, by initially applying a moving average over the number of samples N that were acquired for each engine cycle, thus obtaining a signal called λ_{smooth}.

$$\lambda_{smooth}(k) = \frac{1}{N} \cdot \sum_{i=k-N+1}^{k} \lambda_{confl}(i) \qquad (1)$$

Then, the difference between λ_{confl} and λ_{smooth} was processed by taking an average over 15 engine cycles, in order to isolate the confluence signal oscillations lying in the interesting frequency range.

$$\Lambda(k)=\frac{1}{15}\sum_{i=0}^{14}\left[\lambda_{confl}(k-i\cdot N)-\lambda_{smooth}(k-i\cdot N)\right] \quad (2)$$

According to Nyquist criterion, N should be greater than 4, and possibly around 6~12, since we are searching for frequencies up to twice the engine cycle one. This feature makes the algorithm implementation inside a typical automotive ECU feasible.

Figure 4 shows the results of such signal processing algorithm, by considering a portion of the test shown in Figure 3 (around t=34 [s], while cylinder 1 was controlled at lean AFR values). In particular, the upper plot shows a portion of the UEGO signal measured at the confluence point (λ_{confl}), superimposed to the signal obtained by applying the first moving average (λ_{smooth}), while the lower plot shows the corresponding trend of the final band-pass filtered signal that contains the UEGO signal oscillations (such signal has been called "Λ"). It can be noticed that Λ frequency content is strongly related to the engine cycle frequency (25 Hz @ 3000 rpm) and to its harmonics.

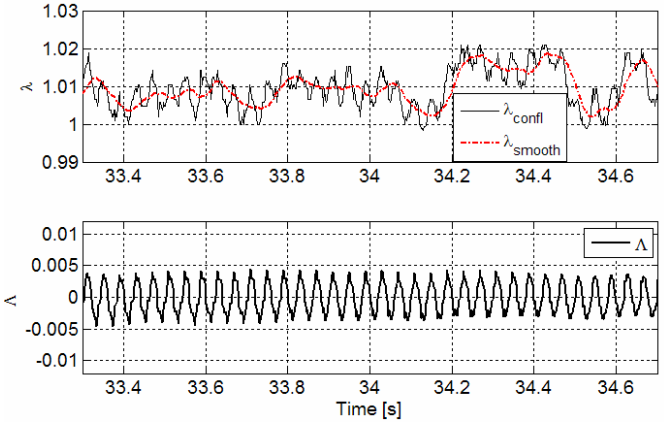

Fig. 4. Signal processing of the confluence UEGO signal. Its oscillations are extracted and isolated in the signal Λ.

Finally, engine cycle and crankshaft rotation frequency components (in terms of amplitude and phase) were evaluated from the signal Λ by using Fourier analysis, which for odd values of N may be expressed as (a similar equation holds for even values of N):

$$\bar{\Lambda}(k)=\Lambda_0+\sum_{n=1}^{\frac{N}{2}-1}\left[\alpha_n\cos\left(2\cdot\pi\cdot n\cdot\frac{k}{N}\right)+\beta_n\sin\left(2\cdot\pi\cdot n\cdot\frac{k}{N}\right)\right]=$$
$$=\Lambda_0+\sum_{n=1}^{\frac{N}{2}-1}\gamma_n\cos\left(2\cdot\pi\cdot n\cdot\frac{k}{N}-\phi_n\right)$$

Where:

$$\Lambda_0=\frac{1}{N}\cdot\sum_{k=k_0}^{k_0+N-1}\Lambda(k)\approx 0$$

$$\alpha_n=\gamma_n\cdot\cos\phi_n\approx\frac{2}{N}\cdot\sum_{k=k_0}^{k_0+N-1}\Lambda(k)\cdot\cos\left(2\cdot\pi\cdot n\cdot\frac{k}{N}\right) \quad (3)$$

$$\beta_n=\gamma_n\cdot\sin\phi_n\approx\frac{2}{N}\cdot\sum_{k=k_0}^{k_0+N-1}\Lambda(k)\cdot\sin\left(2\cdot\pi\cdot n\cdot\frac{k}{N}\right)$$

The second step was then to generate a pseudo-ideal UEGO signal (called "L") composed of the individual cylinder AFR signals, each of them windowed during that specific cylinder exhaust stroke, as shown in Equation (4):

$$L(\theta)=\begin{cases}l_1=\lambda_1-\bar{\lambda}_{confl},\ \ if\ \ \theta\in\left[0;\frac{\pi}{2}\right[\\ l_3=\lambda_3-\bar{\lambda}_{confl},\ \ if\ \ \theta\in\left[\frac{\pi}{2};\pi\right[\\ l_4=\lambda_4-\bar{\lambda}_{confl},\ \ if\ \ \theta\in\left[\pi;\frac{3\pi}{2}\right[\\ l_2=\lambda_2-\bar{\lambda}_{confl},\ \ if\ \ \theta\in\left[\frac{3\pi}{2};2\pi\right[\end{cases} \quad (4)$$

The firing order for the engine under study is 1-3-4-2. $\bar{\lambda}_{confl}$, λ_1, λ_3, λ_4 and λ_2 are to be considered as cycle mean values of the corresponding signals (measured UEGO signal at confluence section, and at each cylinder exhaust runner).

The Fourier series expansion of the signal L is given by:

$$L(\theta)=L_0+\sum_{n=1}^{\infty}\left[a_n\cdot\cos(n\cdot\theta)+b_n\cdot\sin(n\cdot\theta)\right]=$$
$$=L_0+\sum_{n=1}^{\infty}c_n\cdot\cos(n\cdot\theta-\psi_n)$$

Where:

$$L_0=\frac{1}{2\pi}\cdot\int_0^{2\pi}L(\theta)$$

$$a_n=c_n\cdot\cos(\psi_n)=\frac{1}{\pi}\cdot\int_0^{2\pi}L(\theta)\cos(n\cdot\theta) \quad (5)$$

$$b_n=c_n\cdot\sin(\psi_n)=\frac{1}{\pi}\cdot\int_0^{2\pi}L(\theta)\sin(n\cdot\theta)$$

From equations (5) and (4):

$$L_0=\frac{1}{4}\cdot\sum_{i=1}^{4}l_i=\frac{1}{4}\cdot\sum_{i=1}^{4}\lambda_i-\lambda_{confl}=0$$

$$a_1=\frac{l_1-l_3-l_4+l_2}{\pi};\quad b_1=\frac{l_1+l_3-l_4-l_2}{\pi}; \quad (6)$$

$$a_2=0;\quad b_2=\frac{l_1-l_3+l_4-l_2}{\pi};$$

It should be noticed that, since $a_2 = 0$, the phase ψ_2 is either equal to $\frac{\pi}{2}$ or to $\frac{3\pi}{2}$. The systems of Equations (5) and (6) allow solving for amplitudes (c_1, c_2) and phases (ψ_1, ψ_2) of the first two engine cycle harmonics of the pseudo-ideal UEGO signal. The system of equations (3) can instead be used to extract from the lambda signal, measured at the exhaust runners confluence, the amplitudes (γ_1, γ_2) and phases (ϕ_1, ϕ_2) of the corresponding spectrum components. The Λ and L first two Fourier series expansion terms (corresponding to the engine cycle frequency component and its first harmonic) were then compared, to indirectly evaluate the influence of mixing, transport, and measurement system

limited bandwidth on the confluence signal spectrum. An example of the results obtained is shown in the following figure, for a lambda perturbation test similar to the one shown in Figure 3. Both phase (ψ_1 and ϕ_1) and amplitude (c_1 and γ_1) of the engine cycle frequency component of both signals (respectively L and Λ) are shown. It should be noticed that, before plotting the Λ signal, its amplitude was scaled by a factor δ_1, and its phase was shifted by adding a delay β_1 (the values of δ_1 and β_1 are the ones needed to superimpose the two amplitudes and phases, respectively).

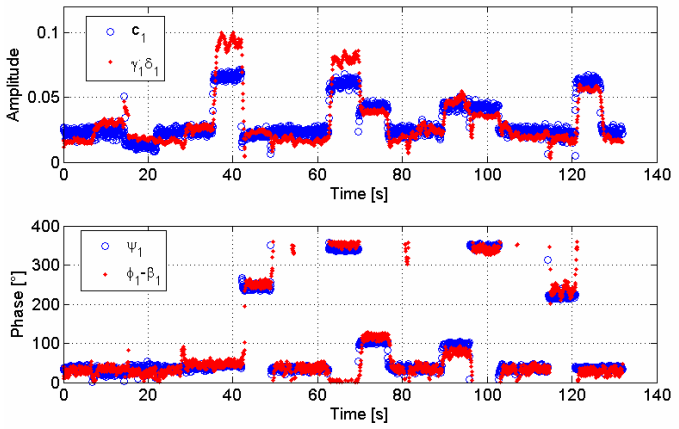

Fig. 5. Cycle frequency component spectrum. Pseudo-ideal UEGO (L) signal amplitude and phase (c_1 and ψ_1), with superimposed measured confluence UEGO signal (Λ) amplitude (γ_1) and phase (ϕ_1).

The fact that the pseudo-ideal UEGO signal cycle frequency content can still be recovered from the measured one, after a scaling and phase shift process, demonstrates the feasibility of the proposed approach, at least for this exhaust configuration (similar results were obtained in other operating conditions, and the methodology has been successfully implemented in the control system of a different engine, as discussed in the next sections). Since we are essentially interested in the phase signal, it should be noted that a simple phase shift allows recovering the necessary information. The quantity β_1 therefore represents the cycle frequency phase delay that should be mapped as characteristic of the specific engine operating point. As it could have been expected, the analysis of the crankshaft rotation frequency (or first harmonic) reveals a lower Signal-to-Noise Ratio (SNR), especially at higher engine speeds. This SNR reduction is probably due to the limited bandwidth of the lambda measuring system, but it appears to be still sufficient to recover the phase information. Finally, the reconstruction of the pseudo-ideal signal amplitude is usually much more affected by noise than the phase reconstruction, as it can be observed in the example of Figure 5, and the identification of robust amplitude attenuation factors (δ_1 and δ_2) cannot be simply performed over the entire engine operating range (also in this case, the SNR is lower for the engine revolution frequency than for the engine cycle one). The control algorithm has therefore been designed without using previously mapped attenuation factor values.

The proposed controller structure is thus straightforward. A standard (and slow) AFR closed-loop controller would keep the engine (or bank) average AFR ($\bar{\lambda}_{confl}$) at its target value, while a faster, individual cylinder controller would perform the following tasks:

- Extract from the measured confluence lambda signal the amplitudes (γ_1, γ_2) and the phases (ϕ_1, ϕ_2) of the engine cycle frequency component and of its first harmonic. Equations (1) through (3).
- Recover pseudo-ideal UEGO signal phases (ψ_1, ψ_2) of the same frequency components, by using ϕ_1, ϕ_2, and previously mapped phase delays β_1 and β_2: $\psi_i = \phi_i - \beta_i(speed, load)$.
- Use measured amplitudes (γ_1, γ_2) and recovered phases (ψ_1, ψ_2) to provide error signals to $2 \cdot Z$ independent individual cylinder closed-loop controllers, which modify injection timing in order to minimize the measured signal amplitudes (γ_1, γ_2). Z stands for the number of cylinders of each engine bank.

The last part of the control algorithm needs to be further clarified. First consider that systems (5) and (6) allow defining a system of 4 equations with 4 unknowns l_1, l_2, l_3, and l_4 (l_i represents the i-th cylinder AFR deviation from the mean lambda value, i.e., the AFR "error"):

$$\begin{bmatrix} 1 & 1 & 1 & 1 \\ 1/\pi & -1/\pi & -1/\pi & 1/\pi \\ 1/\pi & 1/\pi & -1/\pi & -1/\pi \\ 1/\pi & -1/\pi & 1/\pi & -1/\pi \end{bmatrix} \begin{bmatrix} l_1 \\ l_3 \\ l_4 \\ l_2 \end{bmatrix} = \begin{bmatrix} 0 \\ a_1 \\ b_1 \\ b_2 \end{bmatrix} = \begin{bmatrix} 0 \\ c_1 \cdot \cos(\psi_1) \\ c_1 \cdot \sin(\psi_1) \\ c_2 \cdot \sin(\psi_2) \end{bmatrix} \quad (7)$$

If pseudo-ideal amplitudes (c_1, c_2) and phases (ψ_1, ψ_2) could both be reconstructed from measured amplitudes (γ_1, γ_2) and phases (ϕ_1, ϕ_2), the system of Equations (7) would allow recovering individual cylinder AFR fluctuations around the mean value $\bar{\lambda}_{confl}$. As already mentioned, though, the most critical aspect is the reconstruction of pseudo-ideal amplitudes. If one is only interested in minimizing AFR disparity rather than estimating individual cylinder AFR values, it can be demonstrated that measured frequency amplitudes (γ_1, γ_2) can be used instead of reconstructed ones (c_1, c_2), and that two separate individual injection timing closed-loop controllers could minimize AFR disparity based only on measured lambda confluence signal and previously mapped phase delays (β_1 and β_2). In fact, due to the linearity of system (7), each AFR deviation l_i can be thought as being due to two separate contributions: $l_i = l_i^I + l_i^{II}$, defined by:

$$\begin{bmatrix} 1 & 1 & 1 & 1 \\ 1/\pi & -1/\pi & -1/\pi & 1/\pi \\ 1/\pi & 1/\pi & -1/\pi & -1/\pi \\ 1/\pi & -1/\pi & 1/\pi & -1/\pi \end{bmatrix} \begin{bmatrix} l_1^I \\ l_3^I \\ l_4^I \\ l_2^I \end{bmatrix} = \begin{bmatrix} 0 \\ a_1 \\ b_1 \\ 0 \end{bmatrix} \quad (8.1)$$

$$\begin{bmatrix} 1 & 1 & 1 & 1 \\ 1/\pi & -1/\pi & -1/\pi & 1/\pi \\ 1/\pi & 1/\pi & -1/\pi & -1/\pi \\ 1/\pi & -1/\pi & 1/\pi & -1/\pi \end{bmatrix} \begin{bmatrix} l_1^{II} \\ l_3^{II} \\ l_4^{II} \\ l_2^{II} \end{bmatrix} = \begin{bmatrix} 0 \\ 0 \\ 0 \\ b_2 \end{bmatrix} \quad (8.2)$$

Equations (8.1) and (8.2) represent a quite important result. On one hand it has been demonstrated that by reducing cycle and crankshaft revolution frequency amplitudes, also the AFR deviations would be reduced. Another interesting consequence of systems (8.1) and (8.2) is that such amplitudes may be minimized separately, by designing specific controllers, since each of them contributes to the overall AFR deviations with its own pattern.

Finally, only the controller designed to minimize the engine cycle frequency component amplitude will now be described, since the design process is almost identical for the other one. The controller structure is based on the assumption that measured amplitude γ_1 can be used instead of pseudo-ideal amplitude c_1 to recover the coefficients a_1 and b_1 (and therefore the deviations l_i^I, by using equations (8.1)). In fact, if the pseudo-ideal phases (ψ_1, ψ_2) are correctly recovered, the estimated AFR deviations would be related to the real ones by an (unknown) scaling factor (Δ in Equations (9) and (10)). This information (estimated AFR deviations, $\hat{l}_i^I$) is sufficient to feed individual cylinder PI controllers that calculate in real-time individual injection timing corrections, in order to minimize amplitude γ_1.

$$\begin{aligned} a_1 &= c_1 \cdot \cos\psi_1 \rightarrow \hat{a}_1 = \gamma_1 \cdot \cos\left(\phi_1 - \beta_1(speed, load)\right) \approx \Delta \cdot a_1 \\ b_1 &= c_1 \cdot \sin\psi_1 \rightarrow \hat{b}_1 = \gamma_1 \cdot \sin\left(\phi_1 - \beta_1(speed, load)\right) \approx \Delta \cdot b_1 \end{aligned} \quad (9)$$

$$\begin{aligned} \hat{l}_1^I &= \frac{\pi}{4}\left(\hat{a}_1 + \hat{b}_1\right) \approx \Delta \cdot \frac{\pi}{4}\left(a_1 + b_1\right) = \Delta \cdot l_1^I \\ \hat{l}_3^I &= \frac{\pi}{4}\left(-\hat{a}_1 + \hat{b}_1\right) \approx \Delta \cdot \frac{\pi}{4}\left(-a_1 + b_1\right) = \Delta \cdot l_3^I \\ \hat{l}_4^I &= -\frac{\pi}{4}\left(\hat{a}_1 + \hat{b}_1\right) \approx \Delta \cdot \left[-\frac{\pi}{4}\left(a_1 + b_1\right)\right] = \Delta \cdot l_4^I \\ \hat{l}_2^I &= \frac{\pi}{4}\left(\hat{a}_1 - \hat{b}_1\right) \approx \Delta \cdot \frac{\pi}{4}\left(a_1 - b_1\right) = \Delta \cdot l_2^I \end{aligned} \quad (10)$$

The next section will briefly present the experimental setup, before discussing the main results of this work.

4. EXPERIMENTAL SETUP

The Spark Ignition engine used in the real time application phase of this project is a 1.2 liter L4 Port Fuel Injection engine, with firing order 1-3-4-2.

During the tests, all the main engine-load (an eddy- current brake was used for the purpose) actuation parameters were externally controlled in real-time using a Virtual ECU (VECU) developed by this group of research. This device, based on a particular configuration of the dSPACE Real Time System, allows controlling the engine actuators (ignition coils and injectors) in any cylinder, independently of the original ECU. While the availability of such system easily allowed inducing the injection patterns necessary for phase delay identification, it has also been used to test the controller performance in real time, for various engine operating conditions, by implementing the frequency analysis based algorithm using rapid control prototyping techniques. One last aspect is related to the exhaust system layout and to the confluence UEGO installation: It should be noted that the distance between the exhaust valves and the UEGO location is quite different for the various cylinders, for the engine under study. Finally, 4 additional UEGO sensors where installed in each cylinder exhaust runner, close to the exhaust valves. The 4 additional UEGO sensors were not installed for control purposes, but for monitoring and validation purposes only.

5. DISCUSSION AND RESULTS

Two types of experimental tests were performed, respectively for identification and validation purposes:

- Specific injection patterns were applied to the various cylinders, in order to magnify the amplitude of the interesting frequency components, so that the corresponding phase could be identified by analyzing the confluence UEGO signal spectrum. Such type of tests were carried out over a speed range between 1500 and 3500 rpm (with steps of 500 rpm), and a load range between 0.3 and 0.8 bar of intake manifold pressure (with steps of 0.1 bar).
- After having inserted the phase delay maps in the closed-loop controller structure, the algorithm was validated by observing its real-time performance at specific engine operating conditions (see Figure 6).

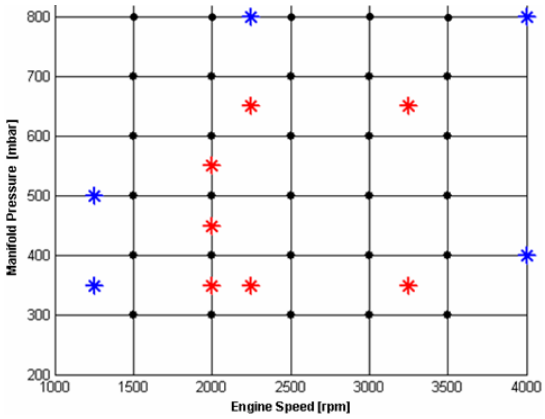

Fig. 6. Identification (˙) and validation (∗) tests.

An example of an identification test is briefly introduced and shown in the following figures. Since the objective of such test is the excitation of the cycle and first harmonic frequency components of the confluence UEGO signal, specific injection time patterns (and corresponding cylinder-by-cylinder AFR distribution) were designed to stimulate such frequency components one at a time, so that the corresponding phase could be isolated and mapped. In particular, two different AFR distributions were used to stimulate each interesting frequency (yielding a total of 4 AFR distributions per test), in order to verify whether the

corresponding unknown phase delay remained constant for that specific engine operating condition, regardless of the type of AFR distribution. Figure 7 shows the 4 interesting parts of the AFR signals measured on each exhaust runner during an identification test performed while the engine was running at 2500 rpm and 0.7 bar of intake manifold pressure. In particular, only steady-state portions of the test were selected to better clarify the identification procedure (they have been separated by vertical dashed lines in Figures 7 and 8). As it can be seen, such 4 portions are relative to 4 different AFR patterns: the first two of such patterns are designed to stimulate mainly the cycle frequency component, while the last two should excite the first harmonic frequency content (the firing order is in fact 1-3-4-2). For example, the first AFR pattern (from t=0 to around t=10 seconds) has been obtained by controlling the various cylinders at the following values: AFR1=14.75; AFR2=AFR3=13.75; AFR4=12.75. The resulting AFR waveform at the confluence point should therefore present a large frequency component equal to the engine cycle frequency, whose phase delay is to be mapped. To better understand the following figure, the cylinder numbers have been reported above the corresponding AFR signals.

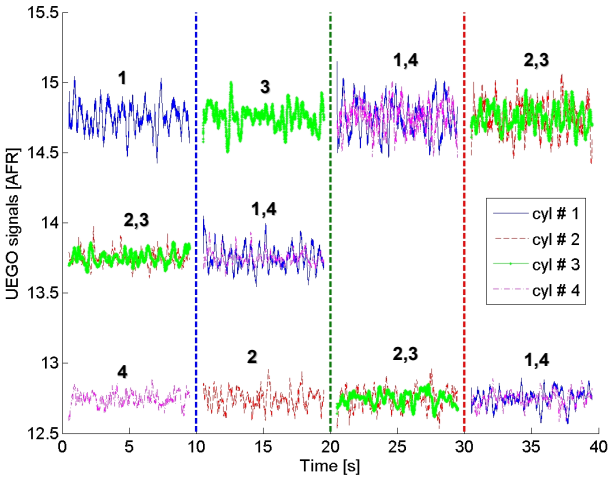

Fig. 7. Identification test at 2500 rpm and 0.7 bar. The four steady-state AFR patterns are shown.

The amplitude and phase that were reconstructed by analyzing the confluence UEGO signal spectrum are shown in Figure 8, for the same test of Figure 7. The amplitude values demonstrate that in fact the first two patterns do excite especially the engine cycle frequency (the corresponding phase trend is also particularly stable during such patterns), while the opposite is true for patterns 3 and 4. The phase trend is strictly related to the corresponding amplitude one: A stable phase value corresponds to higher amplitude, while unstable and oscillating trends can be observed when the corresponding amplitude is very small (as in the first harmonic phase data during the second AFR pattern). The phase delay to be identified is associated with the higher amplitude values (cycle frequency for patterns 1 and 2, and first harmonic for patterns 3 and 4). Of course, there exists a phase shift between pattern 1 and pattern 2 (and between pattern 3 and 4), but its value is known and can therefore be eliminated in order to recover the unknown phase delay.

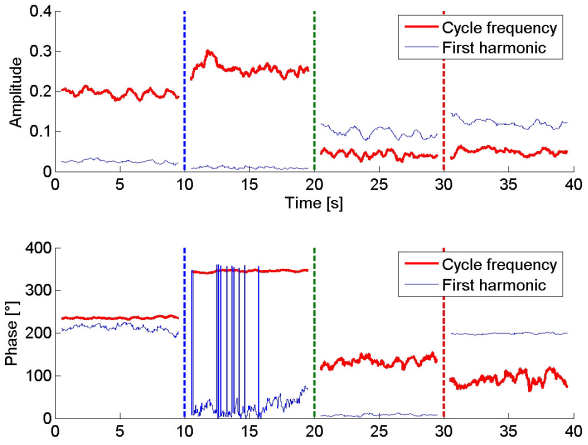

Fig. 8. Identification test at 2500 [rpm] and 0.7 [bar]. Amplitude and phase of the two frequency components induced by four different steady-state AFR patterns.

Finally, an example of the results obtained by running the individual cylinder AFR controller in real time is shown in the following figure.

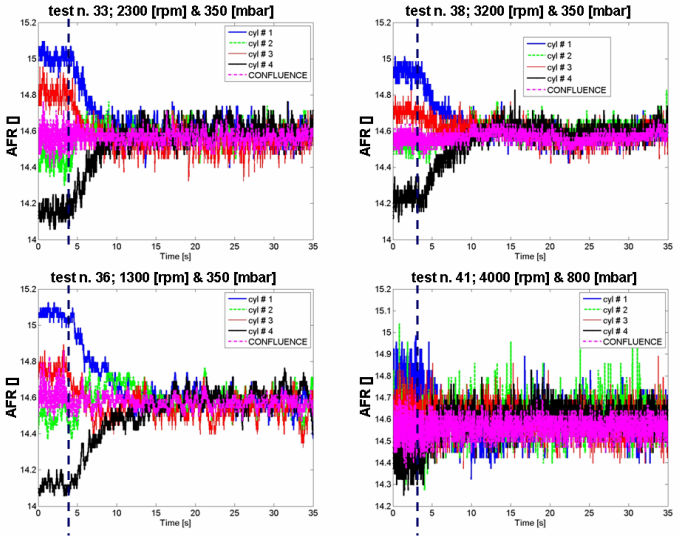

Fig. 9. Example of validation tests. The four cylinder AFR signals are shown, together with the one measured at the confluence point (the only one used by the controller).

These operating points could be critical, due to the relatively high engine speed (tests n. 38 and 41) and low engine load (n. 33, 36, and 38). In fact, both high speed and low load are considered critical because the interesting frequencies increase with increasing engine speed, and the limited sensor bandwidth may then become a problem. Moreover, low load generally signifies low SNR, because of the increased effect of mixing and transport. The tests were carried out by initially controlling the average AFR value of the engine with a slow UEGO-based mean time injection feedback with set-point at AFR=14.60. At around t=4~5 [s], the individual cylinder controller is triggered and starts correcting the various cylinder injection times. The first issue that should be noted is that the average confluence AFR value remains at the constant set-point value (14.60) during and after the transient, even if its oscillations around such value are greatly reduced. Furthermore, the controller performance is

particularly encouraging even for these "critical" speed-load breakpoints. In fact, while the average maximum AFR deviation (mean AFR of the leaner cylinder - mean AFR of the richest one) was as high as 1.00 at the beginning of test n.33, the application of the individual cylinder AFR controller allows reducing such disparity down to 0.1. On one hand, the AFR fluctuations are reduced by 10 times, but even more interesting is the consideration that the controller is able to guarantee AFR disparity below 0.01 lambda (0.1 AFR corresponds in this situation to around 0.007 lambda). Such type of performance was confirmed throughout the entire engine operating region, as shown in Table 1, and the controller was positively tested also under transient conditions. Maximum AFR deviation results by subtracting the richest AFR value from the leanest one (percentage values, evaluated with respect to the average AFR, are reported in the Table), under steady-state conditions.

Table 1. AFR non-uniformity evaluation

MAXIMUM "NATURAL" AFR DEVIATION [%]					
	300	400	500	600	700
1500	6.9	5.2	4.5	3.9	3.0
2000	4.5	3.7	2.9	2.0	1.5
2500	4.5	3.8	2.5	2.7	2.9
3000	4.1	4.1	2.6	2.3	1.4
3500	4.5	4.6	3.0	1.8	2.3
MAXIMUM AFR DEVIATION WITH ACTIVE CONTROLLER [%]					
	300	400	500	600	700
1500	0.7	0.3	0.2	0.2	0.3
2000	0.2	0.4	0.2	0.4	0.4
2500	0.3	0.4	0.3	0.4	0.3
3000	0.4	0.2	0.1	0.3	0.1
3500	1.1	0.2	0.1	0.1	0.3

An example of a transient test is shown in Figure 10. The test consisted of a slow positive and negative load ramp (intake manifold pressure variation between 400 and 800 mbar), while controlling engine speed at a constant value of 4000 rpm (the test lasted around 18 seconds, corresponding to 600 engine cycles at 4000 rpm). The main purpose was to verify the individual cylinder AFR controller ability to deal with (slowly) varying conditions. The controller was triggered before the test start, and it can be observed how it is able to maintain a small cylinder to cylinder AFR deviation (difference between cylinder and confluence measured AFR values) during the test. The same type of performance was observed during other transient speed/load tests.

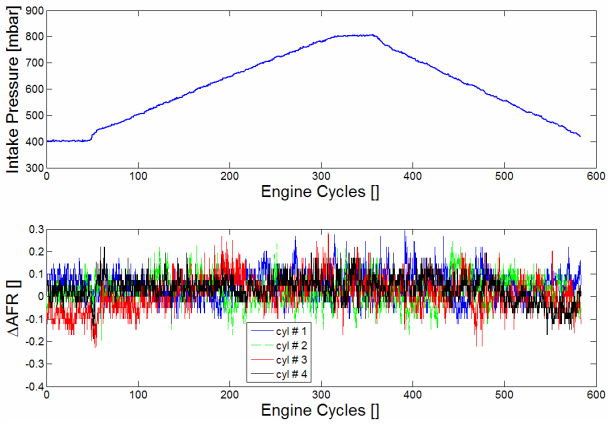

Fig. 10. Example of intake manifold pressure ramp test. ΔAFR is the difference between each cylinder AFR and the one measured at the confluence section.

6. CONCLUSIONS

The paper presents the development and real time application of an original closed-loop individual cylinder AFR control system, based on a spectral analysis of the lambda sensor signal measured at the confluence of the various exhaust runners. The proposed approach has been designed in order to be compatible with on-board application, both in terms of precision and in terms of computational resources. These aspects have been always taken into account during the development of the whole procedure.

The AFR individual cylinder closed-loop controller has been tested in real time, by implementing it in a virtual Electronic Control Unit, using rapid control prototyping techniques. The results observed on a 4 cylinder Spark Ignition 1.2 liter engine are encouraging, since in the investigated engine operating conditions the controller is able to guarantee AFR inequality below 0.01 lambda. The algorithm can be applied without limitations also to an engine mounted on the vehicle, and to other engine configurations.

REFERENCES

Benvenuti, L., Di Benedetto, M. D., Di Gennaro, S., Sangiovanni Vincentelli, A., Individual cylinder characteristic estimation for a spark ignition engine, *Automatica* **39 (2003)** 1157-1169, 2003.

Bush, K. J., Adams, N. J., Dua, S., Markyvech, C. R., Automatic control of cylinder by cylinder air-fuel mixture using a proportional exhaust gas sensor, SAE Technical Paper **940149**, 1994.

Carnevale, C., Hadji, M., Cylinder to cylinder AFR control with an asymmetrical exhaust manifold in a GDI system, SAE Technical Paper **981064**, 1998.

Colvin, A. D., Butler, J. W., Anderson, J. E., Catalytic effects on ZrO2 oxygen sensors exposed to non-equilibrium gas mixtures, *J. Electroanal. Chem.*, **vol. 136**, pp. 179-183, 1982.

Fantini, J., Burq, J. F., Exhaust - intake manifold model for estimation of individual cylinder air fuel ratio, diagnostic of sensor-injector, SAE Technical Paper **2003-01-1059**, 2003.

Fantini, J., Chamaillard, Y., Gouy, F., Peron ,L., Determination of a nonlinear unified, robust individual cylinder air fuel ratio estimator, SAE Technical Paper **2000-01-0262**, 2000.

Grizzle, J. W., Bobbins, K. L., Cook, J. A., Individual Cylinder Air-Fuel Ratio Control with a single EGO sensor, *IEEE Transactions on Vehicular Technology*, **Vol. 40**, N. 1, February 1991.

Hasegawa, Y., Shusuke, A., Komoriya, I., Maki, H., Nishimura, Y., Hirota, T., Individual cylinder air-fuel ratio feedback control using an observer, SAE Technical Paper **940376**, 1994.

Kainz, J. L., Smith, C. J., Individual cylinder fuel control with a switching oxygen sensor, SAE Technical Paper 1999-01-0546, 1999.

Naito, S., Sugiyama, T., Nakamura, Y., . Development of planar oxygen sensor. SAE Technical Paper **2001-01-0228**, 2001.